Effects of Calcium Ion on Ternary Complexes Formed between 4-(2-Pyridylazo)resorcinol and the Two-Zinc Insulin Hexamer†

Niels C. Kaarsholm‡ and Michael F. Dunn*

Department of Biochemistry, University of California, Riverside, California 92521

Received May 12, 1986; Revised Manuscript Received September 18, 1986

ABSTRACT: As a means for probing the microenvironment of zinc in the insulin hexamer and to investigate the effects of calcium ion on the assembly and the structure of the two-zinc insulin hexamer, the thermodynamics and kinetics of the reaction between the chromophoric divalent metal ion chelator 4-(2-pyridylazo)resorcinol (PAR) and zinc–insulin have been investigated over a wide range of conditions. For $[PAR]_0 \gg [Zn^{2+}]_0$ and $[Zn^{2+}]/[In] \leq 0.33$, the reaction leads to the sequestering and ultimate removal of all of the insulin-bound Zn^{2+}; for $[Zn^{2+}]_0 \gg [PAR]_0$, two stable ternary complexes are formed where Zn^{2+} has ligands derived from PAR as well as from hexameric insulin. For $[Zn^{2+}]/[In]$ ratios below 0.33, the equilibrium distribution between the two ternary complexes is dependent on the $[Zn^{2+}]/[In]$ ratio. One of the complexes is assigned to the monoanion of PAR coordinated to Zn^{2+} that resides in a His-B10 site. The other complex is proposed to involve the coordination of (PAR)Zn to the site formed by the α-NH_2 group of Phe-B1 and the γ-carboxylate ion of Glu-A17 across the dimer–dimer interface on the surface of the hexamer. With either PAR or zinc–insulin in large excess, the kinetics of the PAR optical density changes are remarkably similar and biphasic. The faster step is first order in PAR and first order in insulin-bound Zn^{2+} ($k \simeq 3 \times 10^3$ M^{-1} s^{-1}) and involves the formation of an intermediate in which PAR is coordinated to insulin-bound zinc at the His-B10 site. When $[PAR]_0 \gg [Zn^{2+}]_0$, this intermediate is transformed in the slower step into the $Zn^{2+}(PAR)_2$ bis complex and metal-free insulin. When $[Zn^{2+}]_0 \gg [PAR]_0$, the intermediate migrates from the His-B10 site to a different site postulated to be the Phe-B1–Glu-A17 site. The rate of the slower step appears to be limited by the dissociation of the (PAR)Zn complex from the His-B10 site under both conditions. The binding of Ca^{2+} to the Glu-B13 sites of the insulin hexamer stabilizes the intermediate formed at the His-B10 sites in the PAR reaction. Hence, the overall affinity of hexameric His-B10 sites for Zn^{2+} is enhanced when calcium binds to the Glu-B13 site, and therefore, calcium drives the assembly of the two-zinc insulin hexamer.

The three-dimensional structure of the two-zinc insulin hexamer is among the best studied of all proteins (Blundell et al., 1972; Peking Insulin Structure Research Group, 1974; Bentley et al., 1976; Cutfield et al., 1979; Sakabe et al., 1981). The X-ray structure shows the two zinc ions are separated by 15.9 Å and located on the 3-fold symmetry axis in the solvent-filled cavity that runs through the torus-shaped molecule. The two zinc ions reside in octahedral ligand fields, each coordinated by the three histidyl imidazolyl moieties of the His-B10 residues and by three water molecules.

The solution behavior of insulin is known to be complex. The metal-free species exhibits a pH- and concentration-dependent polymerization pattern consisting of monomer, dimer, tetramer, hexamer, and higher aggregation states, all in dynamic equilibrium (Fredericq, 1956; Jeffrey & Coates, 1966; Pekar & Frank, 1972; Goldman & Carpenter, 1974; Jeffrey et al., 1976; Pocker & Biswas, 1981). At pH 7–8, zinc and other divalent metal ions (e.g., Co^{2+}, Cd^{2+}, Ni^{2+}, Mn^{2+}, and Fe^{2+}) strongly shift the equilibrium toward the higher aggregation state(s). When the $[Zn]/[In]$[1] ratio is $\leq$0.33, the hexameric state predominates; at higher ratios, there is a pronounced tendency to form higher aggregates and to crystallize or precipitate (Cunningham et al., 1955; Schlichtkrull, 1956; Fredericq, 1956; Grant et al., 1972; Jeffrey, 1974; Goldman & Carpenter, 1974; Milthorpe et al., 1977).

Chart I: Structural Formulas of PAR and the Mono(PAR)Zn^{II} Complex in Ionization States That Predominate at pH 8.0

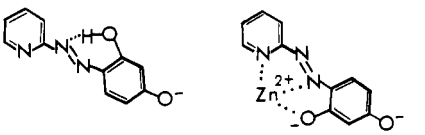

PARH⁻ (PAR)Zn

Earlier work from this laboratory (Dunn et al., 1980) has shown that, in mixtures of zinc and insulin with a $[Zn^{2+}]/[In]$ ratio below 0.33, the reactivity of the zinc ions toward a large excess of the tridentate chelator 2,2′,2″-terpyridine (terpy) is indeed consistent with the assignment of the metal ion environment to that of the crystallographically identified His-B10 sites. Fourier-transform ^{113}Cd NMR experiments with $^{113}Cd^{2+}$-substituted insulin have shown that Cd^{2+} substitution for Zn^{2+} results in the formation of a cadmium–insulin species presumed to be $(In)_6(Cd^{2+})_2Cd^{2+}$; the two classes of high-affinity Cd^{2+} sites have been assigned as His-B10 sites and a new site assigned to the Glu-B13 carboxylates located at the center of the hexamer.[2] Metal ion substitution experiments

† This work was supported by NIH Grant PHS-1-RO1-AM31138 and by a grant-in-aid to N.C.K. from the Danish Natural Science Research Council.

* Address correspondence to this author.

‡ Present address: Novo Research Institute, DK-2880, Bagsvaerd, Denmark.

[1] Abbreviations: In and $(In)_6(Zn^{2+})_2$, insulin monomer and two-Zn hexamer, respectively; terpy, 2,2′,2″-terpyridine; PAR, 4-(2-pyridylazo)resorcinol with unspecified state of ionization; PARHH*, H denotes the hydroxyl proton ortho to the azo group and H* the hydroxyl proton para to the azo group; Tris, 2-amino-2-(hydroxymethyl)-1,3-propanediol.

0006-2960/87/0426-0883$01.50/0

indicate that both $(In)_6(Zn^{2+})_2$ and $(In)_6(Cd^{2+})_2$ are calcium binding proteins and that Ca^{2+} can displace Cd^{2+} from the Glu-B13 site of $(In)_6(Cd^{2+})_2Cd^{2+}$ but not from the His-B10 sites (Sudmeier et al., 1981; Storm & Dunn, 1985). More recently, equilibrium binding studies using $^{45}Ca^{2+}$ have revealed a single high-affinity calcium binding site on the two-zinc insulin hexamer with K_d = 83 μM, and the metal-free insulin species has been shown to bind calcium with an apparent stoichiometry of one site per dimer and K_d = 1.7 mM (Storm & Dunn, 1985).

Since calcium is present in high concentrations in the insulin storage granules (Howell et al., 1975), it is of interest to examine to what extent, if any, the binding of calcium to insulin modulates the complex equilibria between Zn^{2+} and the various insulin species referred to above. In order to probe these interactions, herein we investigate the thermodynamics and kinetics of the interaction between zinc–insulin and the tridentate chelator 4-(2-pyridylazo)resorcinol (PAR) over a wide range of conditions. It is shown that under certain conditions, two types of stable PAR–Zn^{2+}–insulin complexes can be formed. These complexes provide chromophoric indicators which we have exploited as probes to investigate the effect of calcium binding on the interaction between zinc and insulin. It will be shown that calcium drives the assembly of the two-zinc insulin hexamer by enhancing the overall affinity of hexameric His-B10 sites for Zn^{2+}.

Materials and Methods

Materials. PAR and Tris base (Sigma), Chelex 100 (100–200 mesh; Bio-Rad), and $Zn(NO_3)_2$ as the certified atomic absorption standard (Alfa) were purchased and used without further purification. Porcine zinc–insulin (Elanco Division, Eli Lilly) was prepared as described under Methods. All other chemicals employed in these studies were reagent grade or better.

Methods. Metal-free insulin stock solutions with a $[Zn^{2+}]/[In]$ ratio of less than 0.002 were prepared by treatment of solutions of zinc–insulin with Chelex 100 resin as previously described (Dunn et al., 1980). For the determination of insulin concentrations, an extinction coefficient of $\epsilon_{280} = 5.7 \times 10^3$ M^{-1} cm^{-1} was used for the monomer (Porter, 1953). The metal ions of choice were added at the pH of the experiment (typically pH 8.0), and the samples thus prepared were used within the next 4 h. For the results reported herein, no effect of the length of the incubation time in this interval (5 min–4 h) was observed. For the experiments involving the reaction between PAR and mixtures of Ca^{2+} and zinc–insulin (i.e., $[Zn^{2+}]_0 \gg [PAR]_0$; see Results), control experiments wherein each of the components systematically was omitted from the mixture indicate that the Ca^{2+}-induced effects are not the result of a perturbation of the Zn^{2+}–PAR equilibrium per se.

The planar tridentate chelator PAR and its complexes with Zn^{2+} have been described in the literature. Chart I shows structural formulas of the chelator and the (PAR)Zn complex in their relevant ionization states at pH 8.0. Note that as a result of complex formation, the proton from the hydroxyl group ortho to the azo group is displaced. For the free chelator, two macroscopic ionizations with pK's about 6 and 12 are observable. With the assumption that these values represent the microscopic ionizations of the para- and ortho-hydroxyl protons, respectively, according to the pathway

$$\text{PARHH}^* \ (\lambda_{max} = 385 \text{ nm}) \overset{K_1}{\rightleftharpoons} \text{H}^+ + \text{PARH}^- \ (\lambda_{max} = 412 \text{ nm}) \overset{K_2}{\rightleftharpoons} 2\text{H}^+ + \text{PAR}^{2-} \ (\lambda_{max} = 490 \text{ nm})$$

where H* denotes the hydroxy proton para to the azo group, then p$K_1 \simeq 6$ and p$K_2 \simeq 12$, and the following constants have been reported: $[(PAR)Zn]/[PAR^{2-}][Zn^{2+}] \simeq 10^{11}$ M^{-1} [(PAR)Zn λ_{max} = 490 nm]; $[(PAR)_2Zn^{2-}][PAR^{2-}]_2[Zn^{2+}] \simeq 10^{22}$ M^{-2} [$(PAR)_2Zn^{2-}$ λ_{max} = 490 nm]; and $[(PARH^*)Zn^+]/[(PAR)Zn][H^+] \simeq 10^6$ M^{-1} [$(PARH^*)Zn^+$ λ_{max} = 400 nm] (Corsini et al., 1962; Geary et al., 1962; Corsini, 1968; Tanaka, et al., 1968; Ohyoshi, 1983). The following extinction coefficients at pH 8.0 were determined and used for the quantitation of Zn^{2+} content of solutions: $PARH^-$, $\epsilon_{412} = 3.45 \times 10^4$ M^{-1} cm^{-1}; (PAR)Zn, $\epsilon_{490} = 3.5 \times 10^4$ M^{-1} cm^{-1}; and $(PAR)_2Zn^{2-}$, $\epsilon_{490} = 7.1 \times 10^4$ M^{-1} cm^{-1}.

UV–visible spectra were collected with a Hewlett-Packard 8450A UV–visible spectrophotomer. Single-wavelength, rapid kinetic measurements and the kinetic analyses were carried out with a Durrum stopped-flow apparatus and computerized data acquisition system as previously described (Dunn et al., 1979, 1980). For a given set of absorbance vs. time data, the deviation of the absorbance from the final equilibrium value is resolved into a sum of exponentials:

$$\sum_i \Delta OD_i \exp(t/\tau_i)$$

where ΔOD_i and τ_i are the amplitudes and the corresponding relaxation times, respectively, employing the minimum number of phases necessary to reconstruct the experimental time course without systematic deviation.

Results

Static UV–Visible Spectral Analysis of the Interaction between PAR and Zinc–Insulin. Figure 1A compares the UV–visible spectrum of free PAR at pH 8.0 with spectra obtained from mixing the same concentration of chelator with a 10-fold excess of Zn^{2+}, either in the form of free Zn^{2+} or where Zn^{2+} has been premixed with insulin to give a $[Zn^{2+}]/[In]$ ratio of 0.20. At this pH, the spectra of $PARH^-$ and (PAR)Zn exhibit single absorption maxima at 412 and 490 nm, respectively, while the spectrum of the PAR–zinc–insulin mixture has two absorption maxima located at 412 and 495 nm, respectively.

When variable amounts of Zn^{2+}, either as free Zn^{2+} or as zinc–insulin at a fixed $[Zn^{2+}]/[In]$ ratio, are added to sample and reference cuvettes, respectively, containing the same concentrations of PAR, the differences in absorbance at 490 nm (Figure 1B) reveal three distinct regions: (1) region where no difference spectrum is obtained corresponding to [PAR] > (2–3)$[Zn^{2+}]$ (i.e., $[Zn^{2+}] \simeq 0$–8 μM); (2) a region where a constant difference spectrum is obtained corresponding to

[2] Blundell et al. (1972) mention preliminary X-ray diffraction studies of a cadmium–insulin hexamer in which two of the cadmium sites were located in the His-B10 sites, and evidence for a third site in the vicinity of the Glu-B13 carboxylates was mentioned. The structure of $(In)_6(Co^{2+})_2Cd^{2+}$ has now been solved and refined at 2.2-Å spacing (Z. Dauter, G. Dodson, and M. F. Dunn, unpublished results). Two of the Cd^{2+} ions are bound to the His-B10 sites; the remaining Cd^{2+} ion is located within the Glu-B13 cavity. The coordination to the Glu-B13 carboxylates appears highly unusual and involves three identical sites located at the center of the hexamer ~3.5 Å apart in a plane perpendicular to the 3-fold symmetry axis. The electron density map shows that each site has approximately one-third occupancy. Hence, either the structure is disordered or a single Cd^{2+} ion shuttles back and forth among the three sites on a time scale that is rapid relative to the time scale on which the diffraction data are collected. At each site, a pair of Glu-B13 carboxylates from different dimers is positioned to coordinate the metal ion.

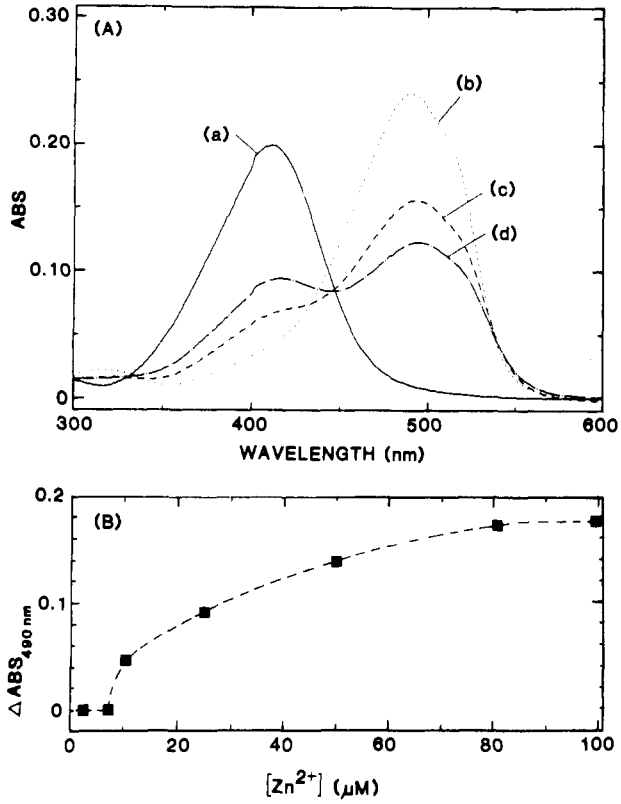

FIGURE 1: (A) UV–visible spectra at pH 8.0 of (—) 6 μM PAR (a), (···) 6 μM PAR + 60 μM Zn^{2+} (b), (- - -) 6 μM PAR + (60 μM Zn^{2+}, 300 μM insulin) (c), and (–·–) 6 μM PAR premixed with 60 μM Zn^{2+}, 300 μM insulin, and 5 mM Ca^{2+} (d). All concentrations refer to final conditions after mixing. (B) Difference absorbance at 490 nm, measured at pH 8.0 after 30 s. Sample cell, 20.5 μM PAR + variable $[Zn^{2+}]$; reference cell, 20.5 μM PAR + same variable $[Zn^{2+}]$, premixed with insulin to give a fixed $[Zn^{2+}]/[\text{insulin}]$ ratio of 0.25.

$[Zn^{2+}] > (4–5)[PAR]$ (i.e., $[Zn^{2+}] > 80$ μM); (3) an intermediate region where the difference spectrum is very sensitive to the $[Zn^{2+}]/[PAR]$ ratio (i.e., $[Zn^{2+}] \simeq 8–80$ μM).

The region of no difference spectrum undoubtedly represents a situation where Zn^{2+} has been sequestered and removed from the insulin hexamer by the 2–3-fold excess of PAR present. The spectrum of this complex is indistinguishable from that of the $(PAR)_2Zn^{2-}$ complex. Under these conditions, a 2–3-fold excess of PAR over insulin-bound Zn^{2+} provides a thermodynamic drive that is sufficient to convert all of the Zn^{2+} to the $(PAR)_2Zn^{2-}$ complex. At the other extreme, the spectral changes saturate at a 4–5-fold excess of insulin-bound zinc over PAR, and the spectrum of the complex (viz., spectrum c in Figure 1A) is characterized by a $\lambda_{max} = 495$ nm with a shoulder located at 412 nm. According to the simple equilibrium PAR + zinc–insulin ⇌ PAR–zinc–insulin, if the spectral change is saturated, then the residual absorbance at 412 nm cannot be due to free PAR. This suggestion was qualitatively confirmed by an experiment where a solution of zinc–insulin ($[Zn^{2+}]/[In] = 0.5$) at pH 8.0 was treated with PAR at a $[PAR]/[Zn^{2+}]$ ratio = 1 and passed over a Sephadex G-100 column in 0.05 M Tris-HC buffer, pH 8.0. The major protein fraction was found to have a $[Zn^{2+}]/[In]$ ratio of about 0.3. This fraction elutes at a volume corresponding to M_r ~36 000, is pink in color, and gives a UV–visible spectrum similar to spectrum c of Figure 1A with peaks at 412 and 495 nm due to bound PAR. When taken together with the finding by equilibrium dialysis that metal-free insulin does not bind PAR, these results establish that the 412- and 495-nm spectral bands which characterize solutions of an excess of zinc–insulin over PAR represent ternary complexes in which Zn^{2+} has ligands derived from the chelator as well as from hexameric insulin. The spectral changes are nearly saturated when there is a 4-fold excess of zinc–insulin (i.e., >90% of the chelator is bound). Under these conditions, the lower limit of the overall affinity constant for the interaction between free PAR and the zinc–insulin system is estimated as $K > (20.5 \times 0.9\ \mu M)/[(20.5 - 20.5 \times 0.9)(82 - 20.5 \times 0.9)\ \mu M^2] = 1.4 \times 10^5\ M^{-1}$ (cf. Figure 1B). Finally, the intermediate region of the absorbance curve in Figure 1B, where the concentration of chelator approaches that of insulin-bound zinc, must represent a mixture of free (PAR)Zn and $(PAR)_2Zn^{2-}$ complexes in equilibrium with the PAR–zinc–insulin species.

The peaks at 412 and 495 nm could simply represent the mono- and dianion forms, respectively, of PAR bound in a single mode to zinc–insulin. Alternatively, these bands could be the result of two distinct classes of binding sites of comparable affinity; since they reside on the same molecule, i.e., the insulin hexamer, the relative number of these sites is fixed. Therefore, the dependence of the distribution of the two complexes on the $[Zn^{2+}]/[In]$ ratio, as measured by the absorbance at 412 and 490 nm, was studied in experiments where a fixed amount of Zn^{2+} is mixed with variable amounts of

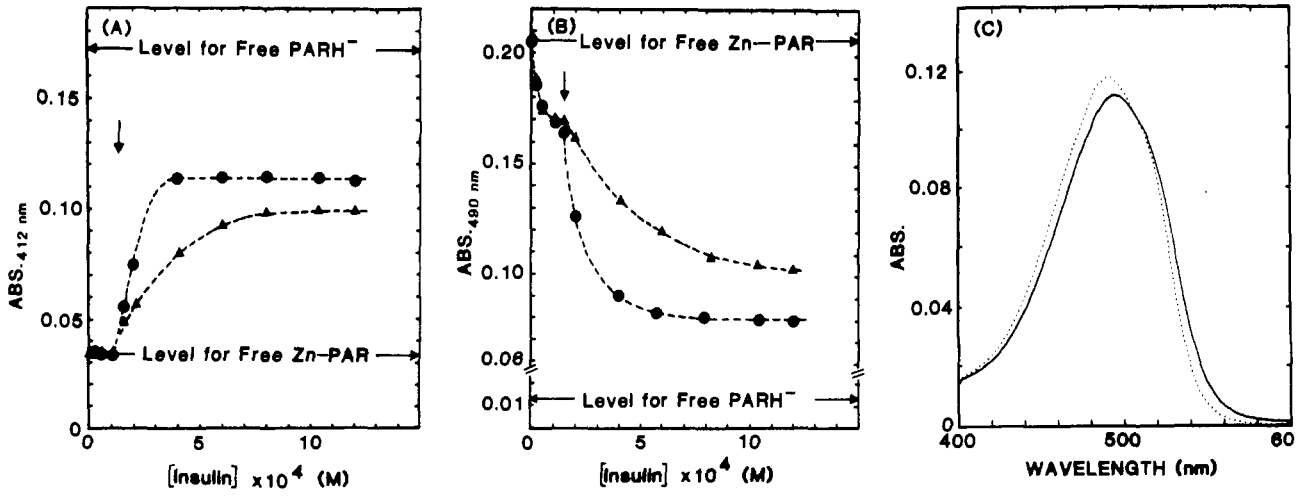

FIGURE 2: Absorbance at (A) 412 nm and (B) 490 nm of solutions at pH 8.0 where 5 μM PAR is added to 50 μM Zn^{2+} premixed with variable concentrations of insulin with (●) and without (▲) 5 mM Ca^{2+}. The vertical arrows indicate a stoichiometry of 2 Zn^{2+} per insulin hexamer. (C) UV–visible spectra at pH 8.0 following addition of 3 μM PAR to 30 μM Zn^{2+} (···) and to a mixture of 30 μM Zn^{2+} and 10 μM $(In)_6(Co^{3+})_2$ (—). (All concentrations refer to conditions after mixing.)

insulin and allowed to equilibrate with a trace of PAR at pH 8.0 before the UV–visible spectra are measured (Figure 2A, B). To compare with the corresponding free (PAR)Zn complex (cf. Figure 1), the absorbance at 490 nm rather than at the λ_{max} (495 nm) is shown in Figure 2B.

At $[Zn^{2+}]/[In]$ ratios greater than 0.33, i.e., more than two Zn^{2+} ions per putative insulin hexamer, the absorbance at 412 nm is indistinguishable from that of a free (PAR)Zn complex under the same conditions, whereas the corresponding absorbance at 490 nm decreases as the $[Zn^{2+}]/[In]$ ratio is decreased to a value approaching 0.33. This result indicates that under these conditions, only the ternary complex absorbing at 495 nm is present at equilibrium.

A further decrease in the $[Zn^{2+}]/[In]$ ratio to values below 0.33 leads to a progressive appearance of the 412-nm ternary complex at the expense of the 495-nm complex in a pattern that approaches saturation at very low levels of the $[Zn^{2+}]/[In]$ ratio. This result implies that the two peaks cannot simply represent an equilibrium between the mono- and dianion of PAR bound to zinc–insulin in a single mode; hence, the interaction must involve at least two classes of sites.

The existence in solution of two (identical) high-affinity zinc sites on the insulin hexamer, i.e., the crytallographically identified His-B10 sites, has been demonstrated (Fredericq, 1956; Grant et al., 1972; Milthorpe et al., 1977; Dunn et al., 1980; Sudmeier et al., 1981). Since a large excess of insulin relative to Zn^{2+} must favor binding to these sites, we assign the 412-nm-absorbing species to the ternary complex in which the monoanion of PAR is coordinated to Zn^{2+} residing in the His-B10 site. Consequently, the 495-nm-absorbing species must be a ternary complex in which (PAR)Zn is coordinated to some other site on the hexamer molecule.

These assignments are strongly supported by an experiment in which a 10 μM sample of a purified preparation of exchange-inert $(In)_6(Co^{3+})_2$ [prepared according to Storm & Dunn (1985)] was mixed with 30 μM Zn^{2+} and allowed to react with 3 μM PAR at pH 8.0 for 20 s before the UV–visible spectrum was measured. As expected and observed, Figure 2C shows that this insulin hexamer, in which the His-B10 sites have been "blocked" by coordination to Co^{3+}, causes a 5-nm red-shift of the absorption maximum relative to that of (PAR)Zn to 495 nm, while the corresponding absorbance at 412 nm is unaffected. This 495-nm band appears identical with that of the 495-nm-absorbing ternary complex.

The pH dependence of the distribution of species in the In–Zn–PAR system (Figure 3) was investigated under conditions of concentration where $[In] > [Zn^{2+}] > [PAR]$. Note that the pH dependence exhibited by the spectrum of the PAR–zinc–insulin mixture is much stronger than that of the (PAR)Zn complex. Thus, for the (PAR)Zn complex, the data at 412 nm adhere to a Henderson–Hasselbach equation for the simple equilibrium $(PARH^*)Zn^+ \rightleftharpoons (PAR)Zn + H^+$ with pK 6.6, whereas for the PAR–zinc–insulin mixture, a much better fit is obtained with the assumption of two simultaneous ionizations of pK 8.1 (cf. Figure 3).

Effect of Calcium on the Equilibrium Distribution between the Ternary Complexes of PAR and Zinc–Insulin. Spectra c and d of Figure 1 compare the effects of calcium on the UV–visible spectrum of the PAR–zinc–insulin mixture. Note that in the presence of calcium, the complexes absorbing at 412 and 495 nm are still present but that calcium appears to preferentially stabilize the 412-nm species, the complex in which PAR coordinates to Zn^{2+} residing in a His-B10 site. At a fixed $[Zn^{2+}]/[In]$ ratio below 0.33, the Ca^{2+} effect is saturable and independent of the order of mixing of the components; i.e., the full effect can be produced either by the addition of Ca^{2+} to the mixture of the ternary complexes or by the premixing of calcium and the zinc–insulin species before reaction with PAR.[3]

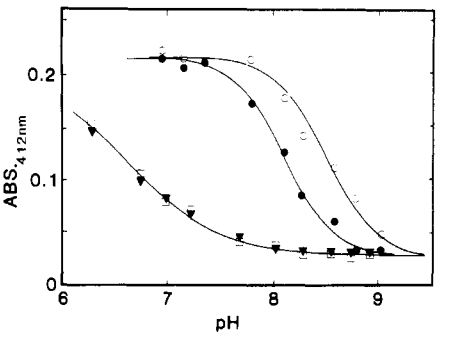

FIGURE 3: pH dependence of the absorbance at 412 nm following addition of 10 μM PAR to solutions of (▼) 100 μM Zn^{2+}, (□) 100 μM Zn^{2+} + 2 mM Ca^2, (●) 100 μM Zn^{2+} + 500 μM insulin, and (○) 100 μM Zn^{2+} + 500 μM insulin + 2 mM Ca^{2+}. Concentrations refer to conditions after mixing. The solid curves are calculated by assuming either one ionization, $OD = [OD_b + OD_a 10^{pK-pH}]/[1 + 10^{pK-pH}]$, or two simultaneous ionizations, $OD = [OD_b + OD_a 10^{2(pK-pH)}]/[1 + 10^{2(pK-pH)}]$, where OD_a and OD_b are the high and low plateau values, respectively. For free Zn^{2+}, a single pK of 6.6 is obtained with and without Ca^{2+}, whereas for zinc–insulin two pK's of 8.1 are obtained in the absence of Ca^{2+} and two pK's of 8.5 in the presence of Ca^{2+}.

The presence of Ca^{2+} was found to affect the distribution of ternary complexes in mixtures of variable $[Zn^{2+}]/[In]$ ratio (Figure 2). For $[Zn^{2+}]/[In]$ ratios above 0.33 at pH 8.0, Ca^{2+} has little or no influence on the product formed in the reaction between PAR and an excess of insulin-bound zinc.[4] As the value of the $[Zn^{2+}]/[In]$ ratio approaches a stoichiometry corresponding to two or fewer zinc ions per putative hexamer, a pronounced effect of Ca^{2+} is observed in which the complex absorbing at 412 nm is stabilized in an "all or none" (highly cooperative) fashion relative to the more gradual transition observed in the absence of calcium (cf. Figure 2A,B). These results clearly indicate that calcium binding to insulin affects the degree of cooperativity in the interaction between zinc and insulin.

Calcium was found to affect the pH dependence of the distribution between the ternary complexes (viz., Figure 3). As is the case also in the absence of Ca^{2+}, the pH-dependent disappearance of the complex absorbing at 412 nm is governed by two simultaneous ionizations, but Ca^{2+} shifts the apparent pK value for this transition from 8.1 to 8.5.

Kinetics of the Reaction between PAR and the Zinc–Insulin System. As documented in Figure 1B, reaction conditions where $[Zn^{2+}]/[In] \leq 0.33$ and $[PAR]_0 \gg [Zn^{2+}]_0$ lead to the sequestering and ultimate removal of insulin-bound zinc and the formation of the free $(PAR)_2Zn^{2-}$ complex. The kinetics of this reaction were followed at 530 nm in the stopped-flow apparatus.

Under conditions where $[Zn^{2+}]/[In] \leq 0.33$ and $[PAR]_0 \gg [Zn^{2+}]_0$, the PAR optical density changes are biphasic in appearance (with relaxation rate constants $1/\tau_1 > 1/\tau_2$). Figure 4A,B shows that $1/\tau_1$ increases linearly with increasing [PAR], while $1/\tau_2$ is independent of [PAR]. The sum of the amplitudes for the fast and slow steps (i.e., the total amplitude)

[3] In separate experiments, it was established that under the conditions employed the presence of Ca^{2+} per se does not affect the equilibrium between PAR and Zn^{2+} (data not shown).

[4] This result is confirmed by the absence of any observable effect of Ca^{2+} on the experiment shown in Figure 2C where substitution-inert $(In)_6(Co^{3+})_2$ is reacted with a trace of PAR in the presence of Zn^{2+}.

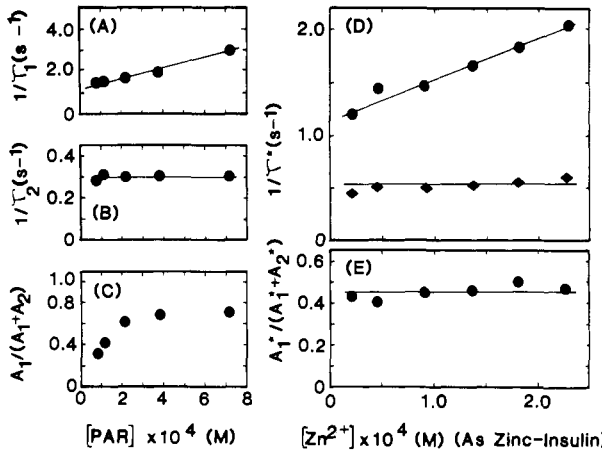

FIGURE 4: Concentration dependencies of the observed reciprocal relaxation times (A and B) and amplitudes (C) for the biphasic reaction of a variable excess of PAR with the zinc–insulin system, i.e., 10 μM Zn^{2+} + 30 μM insulin, at pH 8.0. The slope and intercept values of the best-fit straight line in (A) are 2.5×10^3 M^{-1} s^{-1} and 1.1 s^{-1}, respectively. Panels D and E show the concentration dependencies of the observed reciprocal relaxation times (D) and amplitudes (E) for the biphasic reaction of a variable excess of zinc–insulin (at a fixed $[Zn^{2+}]/[insulin]$ ratio of 0.15) with 6 μM PAR at pH 8.0. The slope and intercept of the best-fit straight line for the concentration dependence of the faster relaxation (●) in (D) are 3.5×10^3 M^{-1} s^{-1} and 1.2 s^{-1}, respectively. The slower relaxation in (D) (♦) is essentially concentration independent.

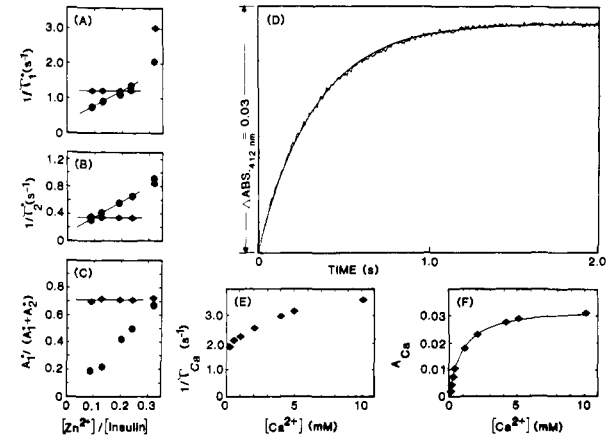

FIGURE 5: Panels A–C show the dependence on the Zn^{2+}/insulin ratio of the apparent reciprocal relaxation times (A and B) and amplitudes (C) characterizing the biphasic time course at 490 nm for the reaction between 80 μM Zn^{2+}, premixed with variable insulin in the (●) absence or (♦) presence of 5 mM Ca^{2+}, and 4 μM PAR at pH 8.0. Panels D–F show the kinetics of the monophasic reaction between variable concentrations of Ca^{2+} and a PAR–zinc–insulin system consisting of 250 μM insulin + 50 μM Zn^{2+} + 5 μM PAR, at pH 8.0. (D) Stopped-flow rapid-mixing kinetic time course at 412 nm for the reaction of 4 mM Ca^{2+} with the PAR–zinc–insulin system. Note that the theoretical, single-exponential time course is overlaid on the experimentally observed time course (noisy trace). Panels E and F show the concentration dependencies of the single observable reciprocal relaxation time ($1/\tau_{Ca}$) and the corresponding amplitude (A_{Ca}), respectively. The best-fit hyperbola in panel F has $A_{Ca,\infty} = 0.33$ and a half-saturation value at $[Ca^{2+}] = 0.8$ mM.

remains constant. However, the fraction of the total OD change occurring in the fast phase increases from approximately 0.30 to a saturated value of about 0.70 (Figure 4C). This kinetic behavior is consistent with a mechanism involving a fast bimolecular step that is coupled to a slower first-order process where both processes contribute about equally to the overall change in optical density.[5]

The rapid mixing of a constant concentration of PAR with increasing concentrations of excess zinc–insulin (at a fixed $[Zn^{2+}]/[In]$ ratio below 0.33) leads to the formation of the mixture of ternary complexes. Under these conditions, the PAR optical density changes (at 490 nm) are also biphasic in appearance. Figure 4D,E summarizes the concentration dependencies of the amplitudes and apparent reciprocal relaxation times for the fast ($1/\tau_1$*) and slow ($1/\tau_2$*) steps of the reaction. As the concentration of zinc–insulin increases, the plot of $1/\tau_1$* vs. [Zn–In] exhibits a linear increase with slope and intercept of 3.5×10^3 M^{-1} s^{-1} and 1.2 s^{-1}, respectively, while over the same concentration range $1/\tau_2$* remains essentially constant at a value of about 0.55 s^{-1}. The sum of the amplitudes for the fast (A_1*) and slow (A_2*) steps remains constant over the range of zinc–insulin concentrations employed, as does the fraction (i.e., 0.4–0.5) of the total OD change occurring in the faster phase $[A_1^*/(A_1^* + A_2^*)]$. Although the separation between the rates is somewhat poorer, this kinetic result is very similar to the one found in Figure 4A–C, where $[Zn^{2+}]/[In] \leq 0.33$ and $[PAR]_0 \gg [Zn^{2+}]_0$.

The dependence of the kinetics of ternary complex formation on the $[Zn^{2+}]/[In]$ ratio was investigated via experiments in which 4 μM PAR is reacted with a solution containing 80 μM Zn^{2+} and variable amounts of insulin at pH 8.0. Under these conditions, the appearance of the two ternary complexes, as measured by the PAR optical density changes at 490 nm, is biphasic. In contrast with the findings referred to below,[5] Figure 5A–C shows that for $[Zn^{2+}]_0 \gg [PAR]_0$, both $1/\tau_1$* and $1/\tau_2$* and the relative amplitude of the fast phase increase significantly as the $[Zn^{2+}]/[In]$ ratio increases in the range below 0.33.

Effect of Calcium on the Kinetics of the Reaction between PAR and the Zinc–Insulin System. Under conditions where zinc–insulin (at $[Zn^{2+}]/[In] < 0.33$) is present in excess over PAR, the binding of Ca^{2+} to insulin perturbs the equilibrium distribution of the ternary complexes (Figures 1–3). The kinetics of the redistribution process were followed at 412 nm by rapidly mixing variable amounts of Ca^{2+} with a PAR–insulin mixture containing 250 μM In, 50 μM Zn^{2+}, and 5 μM PAR. Under these conditions, a single rate process ($1/\tau_{Ca}$) is observed. Figure 5D–F shows a representative kinetic time course together with the concentration dependencies of the apparent reciprocal relaxation time and the corresponding amplitude. Note that the effect of Ca^{2+} is saturable with $1/\tau_{Ca}$ approaching a plateau value of about 4 s^{-1}. The hyperbolic concentration dependence of the OD change shows an apparent half-saturation value of 8×10^{-4} M.

Calcium was also found to abolish the dependence of the biphasic kinetics of ternary complex formation on the $[Zn^{2+}]/[In]$ ratio (Figure 5A–C). Whereas in the absence of Ca^{2+}, the biphasic kinetics of the PAR optical density changes at 490 nm show some variation as the $[Zn^{2+}]/[In]$ ratio changes (in the range below 0.33), inclusion of 5 mM

[5] Note that the zinc–insulin sample employed in Figure 4A–C was prepared as follows: Metal-free insulin and Zn^{2+} were mixed in the ratio $[Zn^{2+}]/[In] = 0.33$ at pH 8.0 and passed over a Sephadex G-100 column in 0.05 M Tris-HCl buffer, pH 8.0. The fractions eluting at a volume corresponding to $M_r \simeq 36000$ and exhibiting a $[Zn^{2+}]/[In]$ ratio of 0.33 were pooled and subsequently used in the stopped-flow experiment. Replicates of the experiment shown in Figure 4A–C with zinc–insulin preparations of lower $[Zn^{2+}]/[In]$ ratio and with no preceding gel filtration step yielded the same values for the rate parameters and relative amplitudes. Similarly, the dependence of rates and relative amplitudes on the $[Zn^{2+}]/[In]$ ratio was investigated in separate experiments in which a fixed amount of Zn^{2+} was premixed with variable amounts of insulin and rapidly mixed with a fixed excess of PAR (relative to Zn^{2+}) at pH 8.0. When the $[Zn^{2+}]/[In]$ ratio is ≤ 0.33, the observed time courses are biphasic, and the ratio of the amplitudes as well as the apparent reciprocal relaxation times for the two phases are invariant (data not shown).

Ca^{2+} with the zinc–insulin mixtures renders both of the apparent reciprocal relaxation times and the amplitude ratio insensitive to this factor.

Discussion

The work in this paper establishes that the very similar overall affinity for Zn^{2+} exhibited by PAR and by insulin at pH 8 renders the coordination of (PAR)Zn to some other site on the hexamer molecule significant even under conditions that otherwise strongly favor binding Zn^{2+} to the His-B10 sites. Thus, it is of particular importance to note that the planar tridentate properties of PAR force the PAR–zinc–insulin complexes into meridional rather than facial coordination. Since the zinc ions of the crystalline two-zinc insulin hexamer reside on the molecular 3-fold axis, formation of ternary complexes with meridional coordination at the His-B10 sites can occur only via rearrangement and/or dissociation of one or more of the histidine ligands (Dunn et al., 1980).

The report of Emdin et al. (1980) provides some clues as to the assignment of the additional (PAR)Zn binding site. On the basis of crystallographic analysis of two-zinc insulin crystals soaked in zinc-containing acetate solutions of varying pH, they detected additional zinc binding at the following sites (listed in order of decreasing occupancy): (1) a pair of Glu-B13 carboxylates; (2) a pair of carboxylates from Ala-B30 and Glu-A4; (3) a pair of His-B5 residues; (4) the γ-carboxyl group of Glu-A17; (5) the pair formed by the α-amino group of Phe-B1 and the γ-carboxyl group of Glu-A17; (6) a single His-B5 residue; and (7) the carboxyl group of Glu-B21. The occupancy of these sites was found to increase with increasing pH (up to 7), while at lower pH (6.0–6.5) zinc binding at the Glu-B13 site in the center of the hexamer still occurred, but binding was reduced at the other sites located on the surface of the hexamer. On the basis of these observations, Emdin et al. (1980) noted that substitution at the Glu-B13 side chains is likely to occur when the hexamer is in solution, and similarly, Blundell et al. (1972) in their earlier review article included the site formed by the α-amino group of Phe-B1 and the δ-carboxyl group of Glu-A17 as an attractive possibility to account for the sharp increase in the zinc binding capacity of insulin with increasing pH in the range 6–8.

Whereas for a (PAR)Zn binding site the Glu-B13 carboxylates in the center of the hexamer appear to be excluded for steric reasons (at least at equilibrium), the site formed by the α-amino group of Phe-B1 and the γ-carboxyl group of Glu-A17 remains a good possibility that could qualitatively account for the complicated pH dependence of the distribution between the ternary complexes observed in Figure 3. Since the formation of two ternary complexes [i.e., $(PARH^*)Zn^+$ coordinated at a His-B10 site and (PAR)Zn coordinated to another site on the hexamer] critically depends on the relative affinity for Zn^{2+} of several chelators, it is important to note that the affinity of PAR for Zn^{2+} per se increases with increasing pH (because the ortho-hydroxyl proton of the resorcinol moiety is released upon chelation; viz., Chart I) and that at pH 9 all of the PAR appears to be bound in the 495-nm-absorbing form. Therefore, the pH-dependent disappearance of the absorbance at 412 nm (cf. Figure 3) is considered to represent the transfer of $(PARH^*)Zn^+$ from a His-B10 site to the other site with concomitant deprotonation to give the (PAR)Zn form. The observation that this process appears to be governed by yet another macroscopic ionization in the pH range 8.1–8.5 (Figure 3) suggests the ionization of the α-ammonium ion of Phe-B1 (which would destroy the ion pair Phe-B1-$NH_3^+\cdots{}^-$OOC-Glu-A17) generates a species competent of binding (PAR)Zn. Consequently, since none of the alternative sites mentioned above would be expected to exhibit pH-dependent changes in this range, we propose that the six pairs of Phe-B1 and Glu-A17 residues, when brought together by dimer–dimer contact in the insulin hexamer, create sites that are capable of competing with the two His-B10 sites for available (PAR)Zn. Although *in the absence of PAR*, the conditions used here (i.e., $[Zn^{2+}]/[In] \leq 0.33$) may render the Phe-B1–Glu-A17 sites of limited importance as zinc binding sites, it should be noted that the packing of molecules in the hexamer leads to numerous close contacts in the region of the Phe-B1 residues (Blundell et al., 1972). Thus, the observation that the covalent addition of phenylthiocarbamyl groups to the α-amino groups of insulin inhibits the zinc-dependent increase in molecular weight of insulin (Marcker, 1960) has been interpreted as due to the sterically impaired formation of hexamers *in combination* with a decreased zinc binding capacity of insulin (Blundell et al., 1972). Of course, this modification also results in the destruction of the stabilizing Coulombic interactions arising from the ion pair.

In earlier work from this laboratory, it has been shown that the two-zinc insulin hexamer is a calcium binding species, and the Glu-B13 carboxylates located at the center of the hexamer have been proposed as the site of Ca^{2+} binding (Sudmeier et al., 1981). More recently, equilibrium binding studies using $^{45}Ca^{2+}$ have revealed the presence of a single high-affinity calcium binding site on the two-zinc insulin hexamer with $K_d = 83\ \mu M$ (Storm & Dunn, 1985). Metal-free insulin also has been shown to bind Ca^{2+} with an apparent stoichiometry of one site per dimer (or three sites per putative hexamer) and an average dissociation constant, K_d, of 1.7 mM (Storm & Dunn, 1985).[2] Already, these results lead to the expectation that the complex set of multiple equilibria connecting the two-zinc insulin hexamer and the insulin monomer are further modulated by calcium binding and that the effects induced by calcium may contain a contribution from the binding of calcium to the two-zinc insulin hexamer per se as well as a contribution resulting from the perturbation of the equilibrium between the (otherwise) metal-free insulin species (Goldman & Carpenter, 1974; Jeffrey et al., 1976; Pocker & Biswas, 1981). On that line, we note that the introduction of PAR constitutes a minor perturbation of the equilibrium between Zn^{2+} and insulin for $[Zn^{2+}] \gg [PAR]$ (viz., Figures 2 and 3).

The kinetics of the reaction between zinc–insulin and another planar tridentate chelator, i.e., 2,2′2″-terpyridine (terpy), have been investigated previously (Dunn et al., 1980). Under conditions where $[terpy]_0 \gg [Zn^{2+}]_0$ and $[Zn^{2+}]/[In] \leq 0.33$, the reaction was found to be biphasic, and a mechanism was proposed in which the fast step involves the coordination of chelator (che) to the protein-bound zinc ion followed by the slow, rate-limiting dissociation of chelator-coordinated zinc ion from the protein (P) and the rapid coordination of a second chelator molecule to give the bis complex $(Che)_2Zn^{2+}$:

$$che + (H_2O)_3Zn^{2+}P \overset{fast}{\rightleftharpoons} (che)Zn^{2+}P + 3H_2O \quad (1)$$

$$(che)Zn^{2+}P \overset{slow}{\rightleftharpoons} (che)Zn^{2+} + P \quad (2)$$

$$che + (che)Zn^{2+} \xrightarrow{fast} (che)_2Zn^{2+} \quad (3)$$

We speculate that the sequestering and removal of zinc ion from the insulin hexamer in vivo by an endogenous chelator occur via a similar pathway and that the kinetics of this process are important for the generation of monomer, the biologically active form of insulin.

The kinetic data presented herein for $[PAR]_0 \gg [Zn^{2+}]_0$ and $[Zn^{2+}]/[In] < 0.33$ (cf. Figure 4A–C and footnote 5) are

in close agreement with those found for terpy under similar conditions and substantiate the minimum mechanism for the overall reaction given above. Furthermore, the fact that very similar values of the second-order rate constants for the binding reaction (eq 1) are obtained for PAR and terpy indicates that this step does not depend on the charge carried by the planar tridentate ligand (1– for PAR and 0 for terpy at pH 8). Still, the second-order rate constant ($\sim 3 \times 10^3$ M^{-1} s^{-1}) is much too slow to be limited by loss of inner-sphere-coordinated water molecules (Eigen & Wilkins, 1964; Dunn, 1975) and therefore must represent some protein-determined step. As has been previously suggested (Dunn et al., 1980), this step could be either the sterically restricted rate of diffusion of chelator to the insulin-bound zinc ion or the rate of inner-sphere substitution from a weak outer-sphere complex with rate-limiting dissociation of a small solvent molecule/ion ligand. Our experiments indicate that the presence of Ca^{2+} has little or no influence on the kinetics of the sequestering and removal of insulin-bound zinc(II) by an excess of PAR.

The biphasic kinetics obtained when either PAR or zinc–insulin is in large excess are remarkably similar (cf. Figure 4) and suggest that despite the different products formed, the rate-limiting step is the same under both sets of conditions. This biphasic behavior is consistent with the formation of a transient species ($\lambda_{max} \simeq 490$ nm) in the fast phase (eq 1), while the formation of the ternary complex absorbing at 495 nm is rate limited by the dissociation of (PAR)Zn from insulin (eq 2). However, the one significant difference between the various kinetic results obtained under the two stes of conditions (Figure 4) is that for $[Zn^{2+}]_0 \gg [PAR]_0$, the rate processes are more degenerate, and this difference becomes particularly clear when the amplitude ratios are considered. Whereas for $[PAR]_0 \gg [Zn^{2+}]_0$ (and for $[terpy]_0 \gg [Zn^{2+}]_0$; Dunn et al., 1980) the spectral changes correspond roughly to the formation of mono and bis complexes, respectively, in each phase, this is evidently not the case for $[Zn^{2+}]_0 \gg [PAR]_0$, where the binding reaction is followed by a redistribution step of considerable complexity. Furthermore, since the similar second-order rate constants observed in Figure 4 indicate that all of the insulin-bound zinc ions exhibit the same or very similar reactivity in the binding step, a physically reasonable formulation of the binding reaction (eq 1) for $[Zn^{2+}]_0 \gg [PAR]_0$ and $[Zn^{2+}]/[In] < 0.33$ could be

$$\begin{array}{l} PARH^- + (H_2O)_3Zn^{2+}P \rightleftharpoons \\ \qquad 3H_2O + H^+ + (PAR)ZnP \quad (\lambda_{max} \simeq 490\ nm) \\ \qquad\qquad \text{fast}\uparrow\downarrow \qquad\qquad (4) \\ \qquad (PARH^*)Zn^+P \ (\lambda_{max} \simeq 412\ nm) \end{array}$$

where the complex formed at the His-B10 site, i.e., (PAR)-Zn^+P, is in rapid equilibrium with the transient species formed in the binding step, and

$$\epsilon_{412}^{PARH^-} > \epsilon_{412}^{(PARH^*)Zn^+P}$$

Although the highly degenerate relaxation spectrum in combination with the complex nature of the redistribution step would seem to preclude a detailed analysis of the rate processes for $[Zn^{2+}]_0 \gg [PAR]_0$, the results presented in Figure 5A–C indicate that *in the absence of* Ca^{2+}, the composition of the zinc–insulin species is dependent on the $[Zn^{2+}]/[In]$ ratio in the range below 0.33, even though all of the insulin-bound zinc ions exhibit the same apparent reactivity in the binding reaction (cf. Figure 4). The direct effect of the binding of Ca^{2+} to insulin (cf. Figure 5D–F) is to bring about a rapid redistribution of the equilibrium between the two-zinc insulin hexamer and the insulin monomer, leading to the transient formation of a relatively high concentration of hexameric His-B10 sites deficient in Zn^{2+} that compete effectively with the Phe-B1–Glu-A17 sites for (PAR)Zn. The rate at which the redistribution occurs is limited only by the off rate of (PAR)Zn from these sites. This explanation is consistent with the interpretation that the binding of calcium to insulin enhances the cooperativity of the formation of two-zinc insulin hexamers.

The demonstration that the two-zinc insulin hexamer forms two distinctly different ternary complexes in the presence of the planar tridentate chelator PAR suggests that the zinc-dependent polymerization pattern of insulin (Jeffrey, 1974; Milthorpe et al., 1977) and also the structural flexibility exhibited by the two-zinc insulin hexamer (Chothia et al., 1983; Reinschedt et al., 1984) are intimately related to the versatility exhibited by Zn^{2+} with respect to "allowed" geometries of coordination (Dunn, 1975). Thus, the presence in the insulin storage granules of high concentrations of Ca^{2+} (Howell et al., 1975) accentuates the need for information on the structural effects induced by calcium binding to the two-zinc insulin hexamer. Nevertheless, it appears that regardless of the microscopic details or pathway of its action, the binding of Ca^{2+} to insulin increases the apparent overall affinity of hexameric His-B10 sites for Zn^{2+} under conditions that maximize the binding of Zn^{2+} to these sites (i.e., $[Zn^{2+}]/[In] < 0.33$; cf. Figure 2). This calcium-induced effect extends to the apparent pH dependence of the stabilization of Zn^{2+} bound to these sites (cf. Figure 3).

Acknowledgments

We thank Dr. Gene Gould for carrying out some of the experiments during the initial phase of the project, and we thank Dr. Steven C. Koerber and James Mason for advice and assistance at various stages of the development of the software and hardware for our rapid kinetics systems.

Registry No. PAR, 1141-59-9; $Zn^{2+}(PAR)_2$, 71016-07-4; Ca, 7440-70-2.

References

Bentley, G. A., Dodson, E. J., Dodson, G. G., Hodgkin, D. C., & Mercola, D. A. (1976) *Nature (London) 261*, 166–168.

Blundell, T., Dodson, G., Hodgkin, D., & Mercola, D. (1972) *Adv. Protein Chem. 26*, 279–402.

Chothia, C., Lesk, A. M., Dodson, G. G., & Hodgkin, D. C. (1983) *Nature (London) 302*, 500–505.

Corsini, A. (1968) *Talanta 15*, 993–995.

Corsini, A., Yih, I. M.-L., Fernando, Q., & Freiser, H. (1962) *Anal. Chem. 34*, 1090–1093.

Cunningham, L. W., Fisher, R. L., & Vestling, C. S. (1955) *J. Am. Chem. Soc. 77*, 5703–5707.

Cutfield, J. F., Cutfield, S. M., Dodson, E. J., Dodson, G. G., Emdin, S. O., & Reynolds, C. D. (1979) *J. Mol. Biol. 132*, 85–100.

Dunn, M. F. (1975) *Struct. Bonding (Berlin) 23*, 61–122.

Dunn, M. F., Bernhard, S. A., Anderson, D.,, Copeland, A., Morris, R. G., & Roque, J.-P. (1979) *Biochemistry 18*, 2346–2354.

Dunn, M. F., Pattison, S. E., Storm, M. C., & Quiel, E. (1980) *Biochemistry 19*, 718.

Eigen, M., & Wilkins, R. G. (1964) in *Mechanism of Inorganic Reactions* (Gould, R. F., Ed.) pp 55–80, American Chemical Society, Washington, D.C.

Emdin, S. O., Dodson, G., Cutfield, J. M., & Cutfield, S. M. (1980) *Diabetologia 19*, 174–182.

Fredericq, E. (1956) *Arch. Biochem. Biophys. 65*, 218-228.
Geary, W. J., Nickless, G., & Pollard, F. H. (1962) *Anal. Chim. Acta 27*, 71-79.
Goldman, J., & Carpenter, F. H. (1974) *Biochemistry 13*, 4566-4574.
Grant, P. T., Combs, T. L., & Frank, B. H. (1972) *Biochem. J. 126*, 433-440.
Howell, S. L., Montague, W., & Tyhurst, M. (1985) *J. Cell Sci. 19*, 395-409.
Jeffrey, P. D. (1974) *Biochemistry 13*, 4441-4447.
Jeffrey, P. D., & Coates, J. H. (1966) *Biochemistry 5*, 489-498.
Jeffrey, P. D., Milthorpe, B. K., & Nichol, L. W. (1976) *Biochemistry 15*, 4660-4665.
Marcker, K. (1960) *Acta Chem. Scand. 14*, 2071-2074.
Milthorpe, B. K., Nichol, L. W. & Jeffrey, P. D. (1977) *Biochim. Biophys. Acta 495*, 195-202.
Ohyoshi, E. (1983) *Anal. Chem. 55*, 2404-2407.
Pekar, A. H., & Frank, B. H. (1972) *Biochemistry 11*, 4013.
Peking Insulin Structure Research Group (1974) *Sci. Sin. (Engl. Ed.) 17*, 779-792.
Pocker, Y., & Biswas, S. B. (1981) *Biochemistry 20*, 4354-4361.
Porter, R. R. (1953) *Biochem. J. 53*, 320-328.
Reinscheidt, H., Strassburger, W., Glatter, U., Wollmer, A., Dodson, G. G., & Mercola, D. A. (1984) *Eur. J. Biochem. 142*, 7-14.
Sakabe, N., Sakabe, K., & Sasaki, K. (1981) in *Structural Studies on Molecules of Biological Interest* (Dodson, G., Glusker, J. P., & Sayre, D., Eds.) pp 509-526, Clarendon Press, Oxford University Press, London.
Schlichtkrull, J. (1956) *Acta Chem. Scand. 10*, 1455-1458.
Storm, M. C., & Dunn, M. F. (1985) *Biochemistry 24*, 1749-1756.
Sudmeier, J. L., Bell, S. J., Storm, M. C., & Dunn, M. F. (1981) *Science (Washington, D.C.) 212*, 560-562.
Tanaka, M., Funahashi, S., & Shirai, K. (1968) *Inorg. Chem. 7*, 573-578.

^{1}H NMR Aromatic Spectrum of the Operator Binding Domain of the λ Repressor: Resonance Assignment with Application to Structure and Dynamics†

Michael A. Weiss,‡,§ Martin Karplus,*,‡ and Robert T. Sauer‖

Department of Chemistry, Harvard University, Cambridge, Massachusetts 02138, Department of Medicine, Brigham and Women's Hospital, Boston, Massachusetts 02115, and Department of Biology, Massachusetts Institute of Technology, Cambridge, Massachusetts 02139

Received June 10, 1986; Revised Manuscript Received September 19, 1986

ABSTRACT: The aromatic ^{1}H NMR resonances of the operator binding domain of λ repressor are completely assigned. Since the resonances of this 23-kilodalton domain are too broad for the application of two-dimensional strategies for sequence-specific assignment, an alternative approach has been used. Assignments are obtained by a combination of one- and two-dimensional NMR methods, by the study of genetically altered domains, and by the biosynthetic incorporation of deuterium labels. The resulting assignments provide sensitive markers for tertiary and quaternary structure. Nuclear Overhauser enhancements demonstrate that the major features of the crystal structure, including the dimer contacts, are retained in solution. The rates of aromatic ring rotation indicate that the globular domain is not rigid; significant barriers to ring rotation are observed only in the dimer contact.

The λ repressor contains two domains, which have distinct functions (Pabo et al., 1979; Sauer et al., 1979). The N-terminal domain recognizes operator DNA, and the C-terminal domain contains strong dimer and higher order contacts. In the intact protein, the two domains are dynamically independent (Weiss et al., 1983). Several other prokaryotic repressors have a similar pattern of domain organization (Platt et al., 1973; Weber & Geisler, 1978; DeAnda et al., 1983; Anderson et al., 1984; Little et al., 1985).

The structure of the N-terminal domain of λ repressor has been determined by X-ray crystallography (Pabo & Lewis, 1982). Consisting of residues 1-92, this domain contains five α-helices, as shown in panel A of Figure 1. The first four helices form a globular domain, and the fifth extends outward to form a dimer contact. In the primary sequence of the N-terminal domain, there are four tyrosines and two phenylalanines (Sauer & Anderegg, 1978). These are shown in panel B of Figure 1. Three tyrosines (Tyr-60, Tyr-85, and Tyr-88) are on the surface of the monomer, and the fourth (Tyr-22) is in the interior of the domain. Both phenylalanines Phe-51 and Phe-76) are internal.

The dimer structure found in the crystal is shown in panel C of Figure 1. The fifth helix of one protomer packs against the symmetry-related helix from the other protomer. These helices are amphipathic, and the packing is primarily hydrophobic. Dimerization alters the environments of the three surface tyrosines. Tyr-88 is buried in the dimer interface, where it stacks against Tyr-88′ from the other protomer. Tyr-60 and Tyr-85 remain on the surface of the dimer but are near side chains from the other protomer.

In this paper we focus on a dimeric fragment consisting of residues 1-102. This fragment contains an additional tyrosine, Tyr-101, which is shown to be in a random-coil state. The aromatic proton resonances are assigned by a combination of one- and two-dimensional NMR methods, by the study of genetic variants, and by the biosynthetic incorporation of

† This work was supported in part by grants from the National Institutes of Health to M.K. (GM-37292) and R.T.S. (AI-15706).
‡ Harvard University.
§ Brigham and Women's Hospital.
‖ Massachusetts Institute of Technology.

0006-2960/87/0426-0890$01.50/0